Reconstruction of Parent Microstructures in TRIP Titanium Alloys

*Alec I. Saville[1], Ben Ellyson[1], A. Eres-Castellanos, Jake T. Benzing[2], Amy J. Clarke[1]

[1]Colorado School of Mines, Golden, CO
[2]National Institute of Standards and Technology, Boulder, CO

*Corresponding author (alec.saville@gmail.com)

Abstract

The metastable β-Ti alloy Ti-10V-2Fe-3Al (wt%) exhibits transformation induced plasticity (TRIP) (or the transformation of the parent β phase to product martensite) and desirable work hardening characteristics. However, the majority of the parent β-Ti microstructure is transformed into α'' martensite during deformation by TRIP, obscuring how parent grain orientations influence the deformation behavior. This work demonstrates the successful reconstruction of parent β-Ti orientations from partially transformed microstructures consisting of remnant β-Ti and α'' martensite. Reconstruction was completed using experimentally derived crystallographic orientation relationships (ORs) and a new, computationally derived OR of equivalent nature. Despite the two ORs being crystallographically *identical,* the reconstructed β-Ti microstructures showed significant differences, showcasing sensitivities that can be present in the reconstruction of parent phases with less common ORs. Regardless of this difference, the demonstrated ability to reconstruct β-Ti microstructures from partially transformed microstructures enables the calculation of orientation specific properties of deformation mechanisms in Ti-10V-2Fe-3Al.

Main

Titanium alloys such as Ti-10V-2Fe-3Al (wt%) (Ti-1023) exhibit transformation induced plasticity (TRIP) when subject to sufficient loading stresses. This requires the initial microstructure to consist of metastable β-Ti to enable the TRIP process, and is achieved via solutionizing heat treatments and rapid quenching [1]. The work hardening and energy absorbing characteristics of alloys like Ti-1023 may be of interest for high strain-rate loading conditions, such as lightweight protective structures [2]. During loading, the metastable body-centered cubic (BCC) β-Ti transforms into orthorhombic α'' martensite via TRIP. The α'' phase is a lower symmetry version of α-Ti produced by β-Ti stabilizers distorting the hexagonal-close-packed (HCP) structure sufficiently to form an orthorhombic crystal structure [3]. A simple hexagonal nanoscale ω phase also forms in Ti-1023 athermally or upon low-temperature aging [2], which further contributes to strengthening of metastable β-Ti alloys [4,5].

A variable amount of β-Ti will transform into α'' martensite depending on strain rate, temperature and chemical stability. Deconvoluting the factors controlling TRIP behavior in Ti-1023 requires information about the parent β-Ti microstructure, especially the orientation of specific deformation systems relative to the loading-axis. However, in many cases a minimal amount of β-Ti (<5 vol%) remains after TRIP. This prevents a coherent understanding of the favorable deformation mechanisms (dislocation slip or TRIP) selected for a given parent grain in response to the parent β-Ti orientation, ω-Ti phase content, and microstructural characteristics.

Metallographic preparation after loading can also transform metastable β-Ti via TRIP, further obscuring such relationships.

One solution is to employ a reconstruction process to recalculate the parent β-Ti grain orientations from product α'' martensite orientations. Such processes require spatially resolved orientation data, information primarily acquired via electron backscatter diffraction (EBSD). Such a process already exists for recalculating parent β-Ti in alloys where HCP α-Ti is the product phase (e.g., Ti-6Al-4V) [6,7]. The parent microstructure is reconstructed using the Burgers orientation relationship (OR). This however, is not applicable to the $\beta \rightarrow \alpha''$ transformation in Ti-1023. Prior work has identified the OR for this transformation is governed by $\{110\}_\beta\|\{001\}_{\alpha''}$ and $< 1\bar{1}1 >_\beta\|< 110 >_{\alpha''}$ [1], but recent work found the OR is close to $\{110\}_\beta\|\{001\}_{\alpha''}$, $\{11\bar{2}\}_\beta\|\{110\}_{\alpha''}$, and $< 1\bar{1}1 >_\beta\|< 110 >_{\alpha''}$ [8].

This work demonstrates the recalculation of parent microstructures for metastable β-Ti alloys. New community-based tools using the MATLAB[1] toolbox MTEX have been developed and enable the processing of orientation data in novel ways [6,9]. These capabilities are implemented here to demonstrate the reconstruction process for alloys with less common ORs and provide insight into the deformation mechanisms of metastable β-Ti microstructures.

For this work, two samples of Ti-1023 were solutionized at 850 °C for 1 hour and water quenched to room temperature, producing a metastable β-Ti microstructure. One sample was left in the as-quenched condition and chilled after heat treatment to prevent room temperature aging. The second was peak-aged (900 sec at 150 °C) to establish the ω-Ti phase [2]. Both samples were loaded to 0.5% strain on an Alliance[1] load frame with a strain rate of 10^{-3} s^{-1} using an ASTM E8 standard subsize-tensile specimen with 25.4 mm gauge length, 6.35 mm width, and 3.175 mm thickness. Strain was measured using an extensometer. Neither sample was loaded to failure to ensure the presence of retained β-Ti and confirm β-Ti orientations from the reconstruction process.

Spatial orientation data for each specimen was carried out via EBSD with a 1 μm step size on a Zeiss Leo[1] 1525 FE-SEM using 20 kV accelerating voltage. In order to evaluate the utility of the new reconstruction process and capture multiple parent β-Ti grains, each EBSD area consisted of dozens of smaller EBSD maps stitched together over a ~3x3 mm area.

EBSD data was processed using the MTEX 5.70 toolbox [10] and the function library ORTools [6]. This latter library enables the analysis of ORs beyond standard MTEX capabilities, and can identify multiple ORs in a material or identify the most accurate OR for a given dataset. All data processing was completed using MATLAB[1] R2020b.

Spatial orientation data of the as-quenched Ti-1023 specimen after deformation is presented in an inverse pole figure (IPF) map in Figure 1a. The loading direction for this specimen is left-to-right across the page. β-Ti still dominates the microstructure, but about 40% of the microstructure has transformed to α'' (Figure 1b). This is despite only 0.5% strain being applied to the specimen. Each grain boundary was calculated in MTEX using a 1.5° misorientation threshold between

---

grains. Any grains less than 50 pixels in width were merged into nearby grains to remove inclusions and a half quadratic filter of 500 was applied to reduce noise.
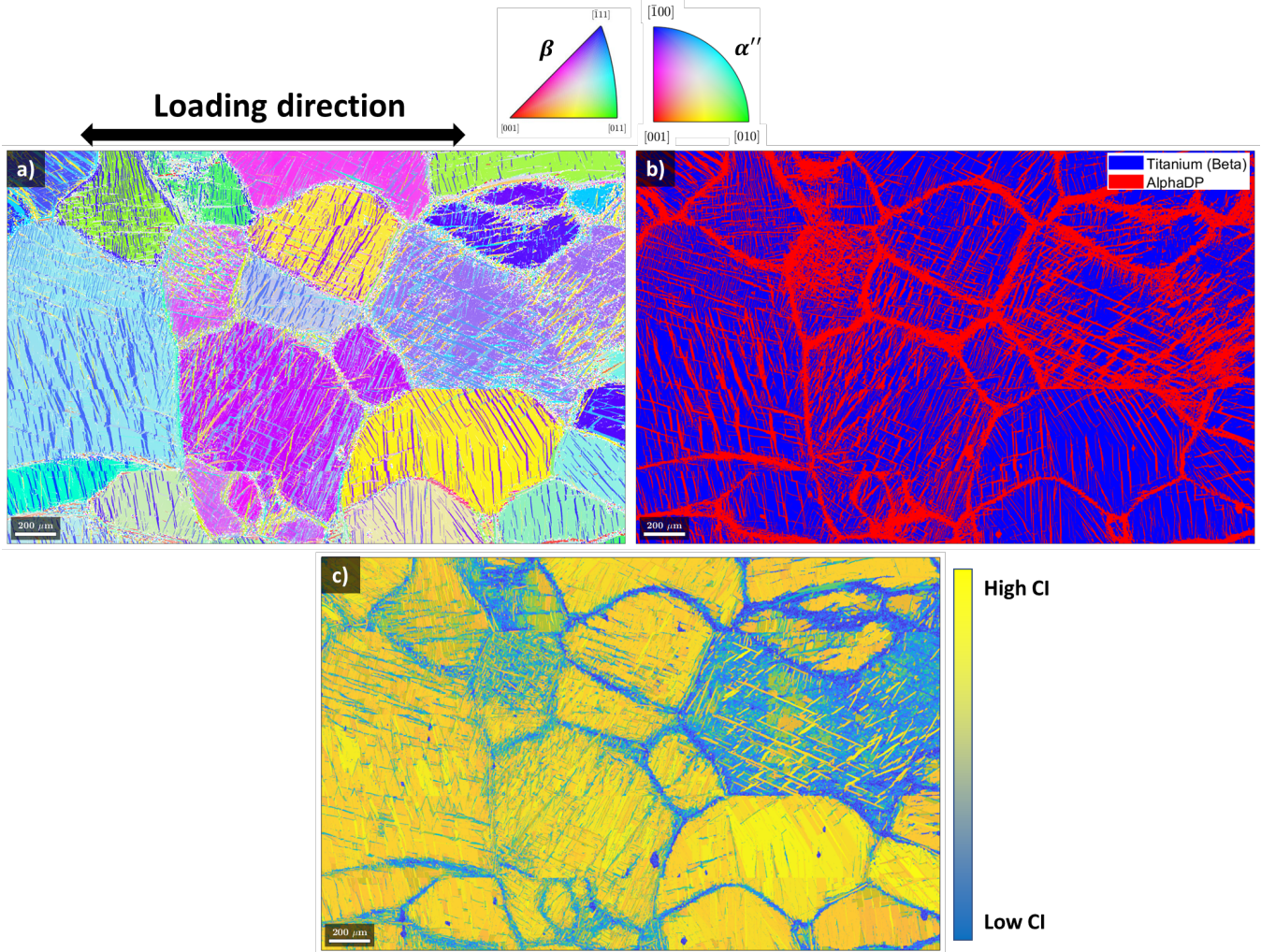

Figure 1: a) IPF map of the as-quenched Ti-1023 specimen after deformation. All orientations are colored with respect to the loading direction (left to right). b) Phase map of the as-quenched microstructure after deformation, illustrating ~40% transformation of β-Ti into α''. c) Confidence index (CI) map illustrating lower CI between parent β-Ti grain boundaries.

Spatial orientation data for the peak-aged Ti-1023 specimen is included in Figure 2a. A comparable amount of intragranular β-Ti transformed into α'' (Figure 1), while less α'' was formed between the parent grains (Figure 2b). Whether this was due to increased noise at grain boundaries in Figure 1c or is truly representative of the microstructure is unknown at this time and is the subject of future EBSD investigations. Regardless, ~30% of the microstructure consists of α''.
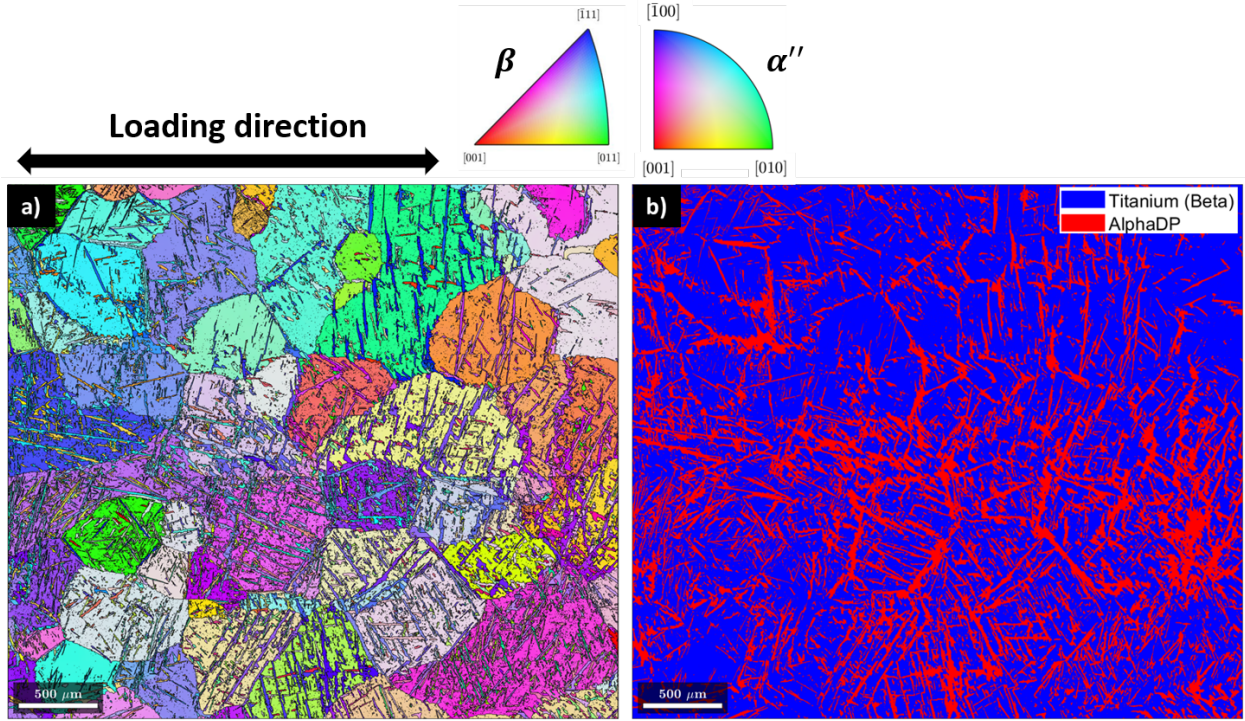
Figure 2: a) IPF map of the peak-aged Ti-1023 specimen after deformation, illustrating partial transformation of the parent β-Ti microstructure. All orientations are colored with respect to the loading direction (left to right) in the page. b) Phase map of the of the microstructural region surveyed in a) containing 30% α''.

Using the crystal symmetries of α'' and β-Ti, the ORTools library can estimate ORs from the post-strain microstructures in Figure 1 and Figure 2. This process includes calculating the parent-product misorientations from crystal symmetries and evaluating the frequency of specific misorientations. Those with the highest frequencies correspond to ORs. Plots illustrating these parent-product misorientations are provided in Figure 3a for the as-quenched specimen, and Figure 3b for the peak-aged specimen. Only one OR was found for both conditions.
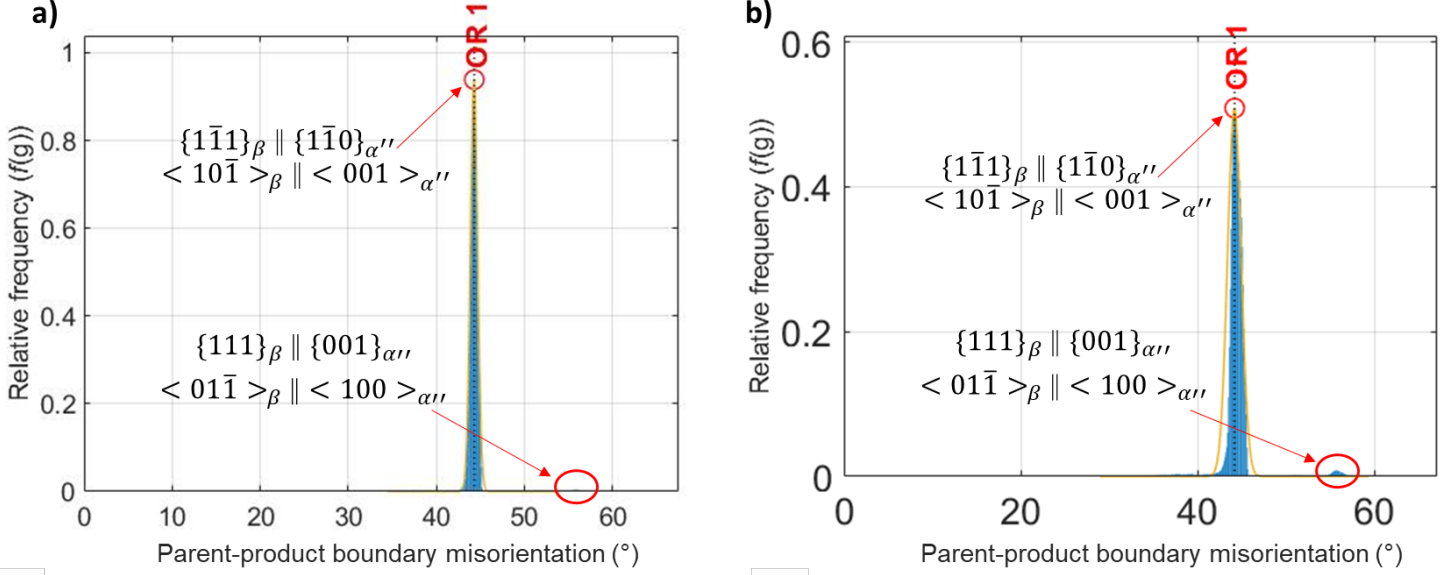
Figure 3: a) Parent-product misorientation histogram of the as-quenched specimen. Note the intensity of the dominant OR almost reaches a relative frequency of 1. A weak second OR is barely visible at ~55.5°. b) Misorientation histogram of the peak-aged specimen illustrating the same dominant OR observed in a). The same weak second OR is also observed at ~55.5°.

Calculating the OR corresponding to the dominant misorientation returns the values in Table 1.

Table 1: $\beta \leftrightarrow \alpha''$ OR as determined by ORTools.

$$\{1\bar{1}1\}_\beta \parallel \{1\bar{1}0\}_{\alpha''}$$
$$< 10\bar{1} >_\beta \parallel < 001 >_{\alpha''}$$

This OR is previously unreported. Most ORs are determined via transmission electron microscopy (TEM) enabling high resolution analysis of the crystallographic alignments. The process employed here is the opposite of traditional OR discovery, where considerable swathes of orientation data are compared crystallographically to identify an optimal OR. It is worth noting *no* other favorable ORs were reported for both specimen conditions, demonstrating a strong preference for the above orientation.

ORTools also returns the angular deviation between the crystallographic orientation given by an OR and the actual orientations in the material. Such misorientations evaluate the accuracy of a computer OR, and hint at aspects of the transformation process (e.g., residual or thermal stress).

For the as-quenched specimen, a 0.22° offset from perfect alignment for the calculated planes, a 0.07879° offset for the calculated directions, and a 45.06° misorientation defining the OR were calculated. The peak-aged specimen meanwhile had a 0.087° misorientation from ideal plane alignment, a 0.067° ideal direction misorientation, and an OR misorientation of 45.12°. This indicates the peak-aged microstructure more closely exhibits the calculated OR. Such findings

5

suggest subtle rotations of the α'' martensite depending on local strain conditions and ω-Ti phase fraction.

A second OR was also observed in Figure 3 at ~55.5° misorientation. This corresponds to an OR of $\{111\}_\beta\|\{001\}_{\alpha''}$ and $< 01\bar{1} >_\beta\|< 100 >_{\alpha''}$. The origins of this OR are unknown at this time, but localized twinning could be present. This OR was not investigated further given its low frequency.

Reconstruction of the parent β-Ti microstructure for both samples was completed via a triple-point grain boundary voting method to validate the new OR [6]. Reconstructions employing the previously reported OR [1] were also completed with the same algorithm for comparison. Calculations using the old OR did not include the most recently reported plane-direction pairs [8].

Within the voting algorithm a range of 2.5°-to-5° was applied for votes on parent grain triple-points, a 70% confidence threshold set for parent grain votes, and a 2.5° threshold declared for growing parent grains after reconstruction. A 3° misorientation threshold between parent grains and a half-quadratic smoothing filter of 50 were applied in generation of subsequent IPF maps. These reconstructions are summarized in Figure 4.
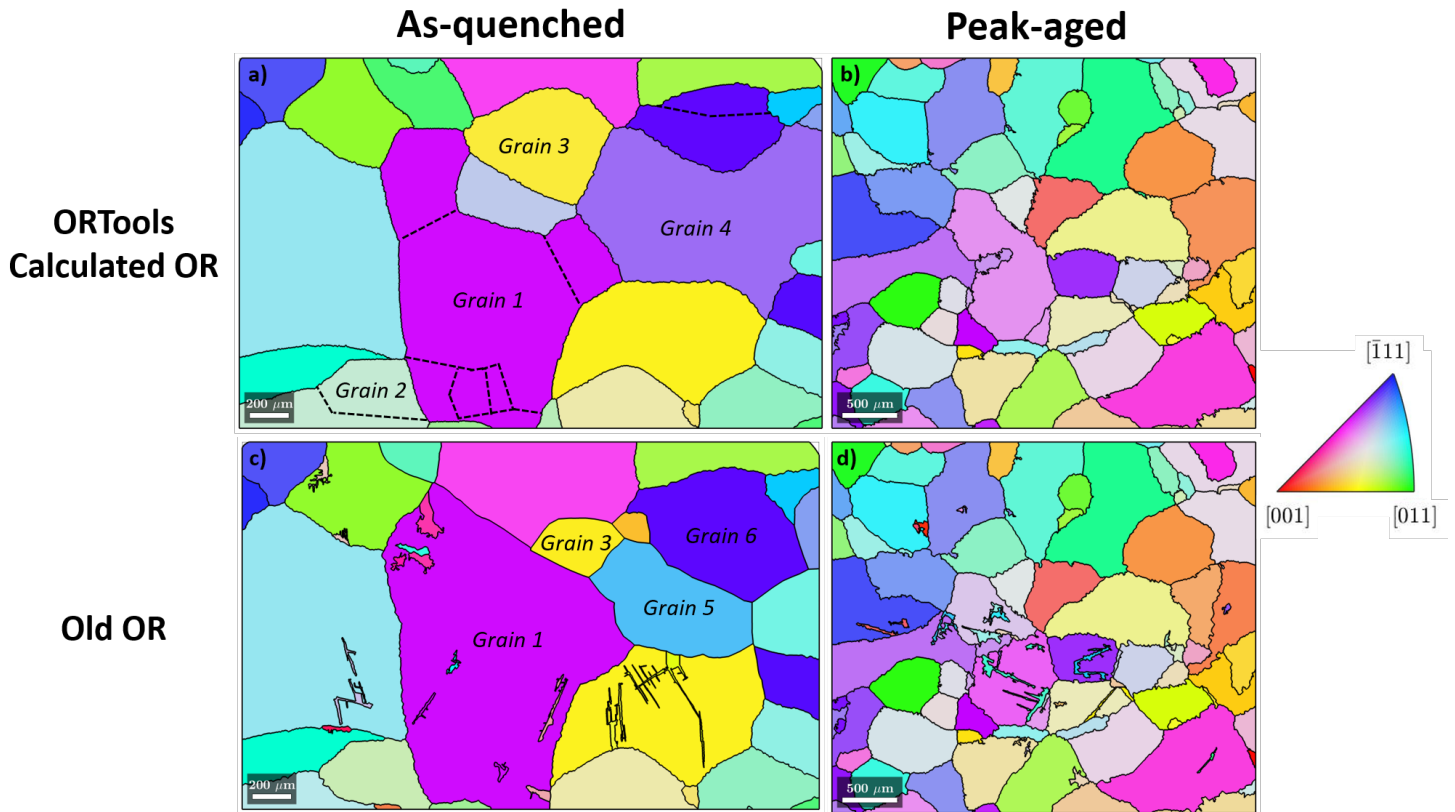

Figure 4: Ti-1023 β-Ti IPF map reconstructions of the as-quenched and peak-aged microstructures seen in Figure 1 and Figure 2. Parent microstructures in a) and b) were calculated using the new OR reported in Table 1, while c) and d) were calculated using the old OR reported for the $\beta \rightarrow \alpha''$ transformation [1]. The new OR demonstrates an overall better reconstruction, though both ORs require further optimization for avoiding incorrect grain merging. All IPF maps are colored with respect to the loading direction (left to right). Specific grains are identified in a) and c) to highlight

significant differences between the two reconstructions. Incorrectly merged grains for the ORTools calculated reconstruction are highlighted by dashed black lines in a).

Figure 4a+b demonstrate the newly calculated OR effectively reconstructs the parent β-Ti microstructure. Parent β-Ti with misorientations less than 3° were incorrectly merged together in Figure 4a+b, but this can be addressed by further processing. The correct grain boundaries are outlined in Figure 4a. This effect was most prominent in the as-quenched specimen, where the grains marked Grain 1 and Grain 2 are artificially expanded. Regardless, all transformed martensite was successfully recalculated into a corresponding parent volume of β-Ti, and even fine β-Ti grains can be clearly observed post-reconstruction.

Figure 4c+d illustrate reconstructed IPF maps employing the old OR for the $\beta \rightarrow \alpha''$ transformation. Interestingly, the old OR struggles to accurately calculate β-Ti grains near the center of the as-quenched microstructure. Grain 1 is further grown incorrectly up the IPF map, and the nearby Grain 3 is drastically reduced in size. The old OR also breaks up the large Grain 4 on the right side of the map into differently oriented β-Ti grains marked Grain 5 and 6. This indicates the old OR was unable to accommodate for the transformation process in these regions, instead reconstructing β-Ti with the closest possible orientations. Thus, the old OR can only recreate ~60% of the as-quenched microstructure compared to ~85% with the new OR. Remnant α'' can also still be observed in Figure 4c, but the majority of martensite has been transformed back to its parent β-Ti orientation.

The peak-aged microstructure in Figure 4d demonstrates a comparable reconstruction accuracy to that of Figure 4b. The incorrectly merged bean-shaped grain in the left-center of Figure 4b is correctly represented using the old OR, however remnant martensite is still present. It is likely the presence of this retained martensite prevented the merger of the bean-shaped grain as was observed in Figure 4b. The reconstructions from both ORs are otherwise similar.

Evaluating the misorientation between the two ORs reveals a surprising discovery. The old and new ORs are in fact, *crystallographically equivalent*. Even with the plane and direction pairs being flipped between the new and old ORs, the same α'' orientations manifest from a given β-Ti orientation. This can be clearly seen in Supplementary Figure 1 (see Supplementary Materials).

This finding begs an obvious question: How can different reconstruction results be produced from the *same* crystallographic relationships? Dissecting the reconstruction process, the variants for each OR were listed in different orders. This was likely due to the different signs of the "seed" orientation used to define each OR (for example, a (101) plane might be listed before the (10-1) plane considering the negative value). Though this appears to be a minor detail, this may have influenced the reconstruction process in greater ways than one would expect.

The triple-point voting algorithm used to reconstruct β-Ti grains in this work evaluates the *most favorable* parent orientation for every pixel. Multiple parent orientations may be equivalent in favorability though, and thus a later step compares the selected orientation to nearby points to validate the chosen reconstruction orientation. However, this process requires a parent orientation value be given to every point before comparison. It is at this step that the difference in reconstructions likely emerges.

For this work, the first *most favorable* parent orientation was selected as they are listed chronologically in MTEX. However, as the two ORs do not chronologically list variant orientations in the same order, equivalently favorable parent orientations may be selected and retained. For example, parent orientation A and C may be favorably equivalent for reconstructing a given α'' lath. However, given the ORs list variants in different orders, the new OR could select parent orientation A and the old OR parent orientation C. This process could occur both locally around α'' martensitic laths and also throughout a parent β-Ti grain if enough points are given the same parent orientation. Thus, the reconstructions would differ.

Given the unusual behavior of these reconstructions, *both* the reconstruction script and data in this study are provided to the greater scientific community at 10.17632/hmr68jfccn.1. This aims to provide transparency regarding the results presented in this work, and showcase nuances in reconstructing EBSD datasets of less-common systems. However, the fact an equivalent OR to that previously found [1] was computationally determined using community methods demonstrates the accuracy of these tools.

Regardless of the aforementioned nuances, successful β-Ti reconstructions enable the quantification of deformation mechanisms in both the as-quenched and peak-aged conditions. This is accomplished by calculating Schmid factors of dislocation slip and other deformation mechanisms in relation to the loading axis. These values can then be compared to the propensity for a specific deformation mechanism within each grain and elucidate how β-Ti orientation influences the deformation behavior during loading. Figure 5 illustrates a $\{110\}_\beta < 1\bar{1}1 >_\beta$ dislocation slip Schmid factor heat map for both the reconstructed as-quenched and peak-aged microstructures using the computationally derived form of the Ti-1023 $\beta \leftrightarrow \alpha''$ OR.
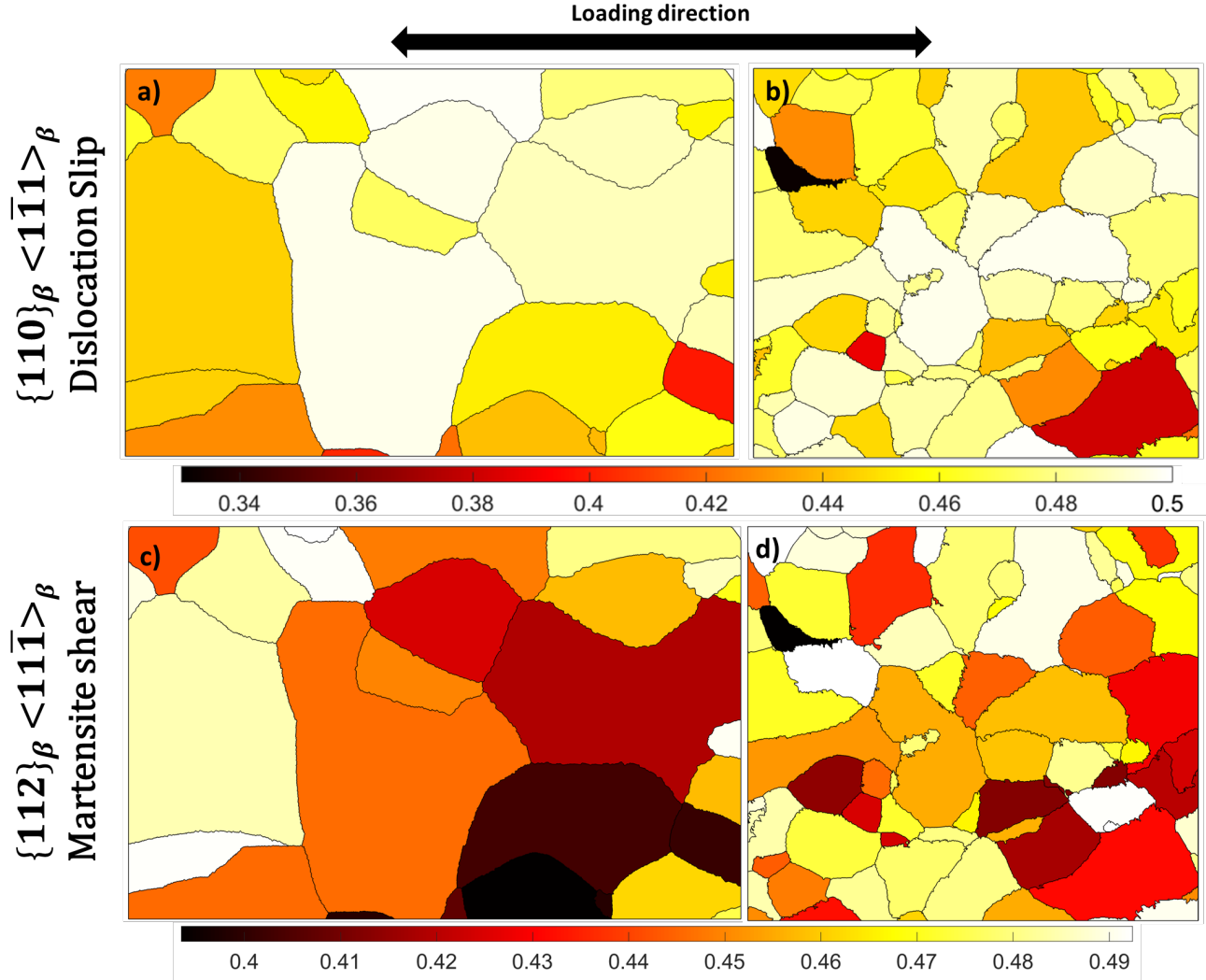
Figure 5: $\{110\}_\beta < 1\bar{1}1 >_\beta$ dislocation slip Schmid factor maps for the reconstructed β-Ti microstructures in the as-quenched a) and peak-aged b) conditions. c) and d) illustrate Schmid factor maps for the $\{112\}_\beta < 11\bar{1} >_\beta$ shear transformation system associated with the $\beta \rightarrow \alpha''$ martensite transformation. Loading direction for the calculation is indicated above the heat maps. Scale is the same as the images seen in Figure 1, Figure 2, and Figure 4.

Both Figure 5a+b demonstrate the as-quenched and peak-aged parent microstructures have similar average Schmid factors for $\{110\}_\beta < 1\bar{1}1 >_\beta$ dislocation slip. Figure 5c + d illustrate the Schmid factors for the $\{112\}_\beta < 11\bar{1} >_\beta$ TRIP martensite system, with the as-quenched microstructure exhibiting slightly lower Schmid factors on average. These values are only ~5-10% lower than those reported for the peak-aged specimen in Figure 5d. It stands to reason an equivalent number of grains should be compared to quantitatively determine the shear favorability for martensite. Regardless, it appears here the establishment of ω-Ti by aging may influence the favorability to activate TRIP over the as-quenched condition. This was not significantly obvious in EBSD maps, indicating the effect is limited and likely dependent on the magnitude of applied stress. No such influence was obvious for dislocation slip.

The Schmid factor is employed here to evaluate the favorability of a projected stress onto specific deformation or transformation systems. This does not convey *if* the specific plane-pair system will be activated, only the geometrical favorability of the system given a grain's crystallographic orientation. This requires the calculation of critical resolved shear stress and knowledge on the activation stresses for the system in question.

This work has demonstrated a new method to implement existing capabilities in reconstructing parent β-Ti microstructures in Ti-1023 containing TRIP α'' martensite. Such a process enables the calculation of orientation dependent deformation properties for parent β-Ti microstructures in Ti-1023. A new, unreported OR was computationally determined for both the as-quenched and peak-aged microstructures but found to be crystallographically equivalent to previously reported values for Ti-1023. Despite this fact, the computationally derived version of the OR more effectively reconstructed the parent microstructure due to differences in computational processing during the reconstruction process. Such a difference highlights the need to test for sensitivities in reconstruction of parent phases, especially as tools available to the scientific community continue to expand in capability. Having demonstrated the ability to reconstruct parent β-Ti microstructures in Ti-1023, the calculation of deformation system Schmid factors can be completed to better understand active deformation mechanisms. Future work aims to expand the application of this reconstruction process to *fully* transformed microstructures to enable further exploration of microstructural evolution during loading of Ti-1023 and related alloys.

Acknowledgements

References

[1] T.W. Duerig, R.M. Middleton, G.T. Terlinde, J.C. Williams, Titanium '80 Science & Technology - Proceedings of the 4th Int'l Conference on Titanium 2 (1980).
[2] B. Ellyson, J. Klemm-Toole, K. Clarke, R. Field, M. Kaufman, A. Clarke, Scripta Materialia 194 (2021) 113641.
[3] F.C. Campbell, Elements of Metallurgy and Engineering Alloys, ASM International, Materials Park, Ohio, 2008.
[4] H. Sun, Y. Liang, G. Li, X. Zhang, S. Wang, C. Huang, Journal of Alloys and Compounds (2021) 159155.
[5] J.Y. Zhang, G.F. Chen, Y.Y. Fu, Y. Fan, Z. Chen, J. Xu, H. Chang, Z.H. Zhang, J. Zhou, Z. Sun, B.L. Shen, F. Sun, Journal of Alloys and Compounds 799 (2019) 389–397.

[6] F. Niessen, T. Nyyssönen, A.A. Gazder, R. Hielscher, ArXiv:2104.14603 [Cond-Mat] (2021).

[7] A.L. Pilchak, J.C. Williams, Metallurgical and Materials Transactions A 42 (2011) 773–794.

[8] C.H. Wang, C.D. Yang, M. Liu, X. Li, P.F. Hu, A.M. Russell, G.H. Cao, J Mater Sci 51 (2016) 6886–6896.

[9] R. Hielscher, T. Nyyssönen, F. Niessen, A.A. Gazder, ArXiv:2201.02103 [Cond-Mat] (2022).

[10] F. Bachmann, R. Hielscher, H. Schaeben, Solid State Phenomena 160 (2010) 63–68.